Published in final edited form as:
Mutat Res. 2011 August 1; 713(0): . doi:10.1016/j.mrfmmm.2011.05.018.

Human induced pluripotent cells resemble embryonic stem cells demonstrating enhanced levels of DNA repair and efficacy of nonhomologous end-joining

Jinshui Fan[a,1], **Carine Robert**[a,1], **Yoon-Young Jang**[b], **Hua Liu**[b], **Saul Sharkis**[b], **Stephen Bruce Baylin**[b], and **Feyruz Virgilia Rassool**[a,*]

[a]Department of Radiation Oncology, University of Maryland School of Medicine, 655 West Baltimore Street, BRB 7-023A, Baltimore, MD 21201, United States

[b]Johns Hopkins University School of Medicine, Department of Oncology, Baltimore, MD 21231-1000, United States

Abstract

To maintain the integrity of the organism, embryonic stem cells (ESC) need to maintain their genomic integrity in response to DNA damage. DNA double strand breaks (DSBs) are one of the most lethal forms of DNA damage and can have disastrous consequences if not repaired correctly, leading to cell death, genomic instability and cancer. How human ESC (hESC) maintain genomic integrity in response to agents that cause DSBs is relatively unclear. Adult somatic cells can be induced to "dedifferentiate" into induced pluripotent stem cells (iPSC) and reprogram into cells of all three germ layers. Whether iPSC have reprogrammed the DNA damage response is a critical question in regenerative medicine. Here, we show that hESC demonstrate high levels of endogenous reactive oxygen species (ROS) which can contribute to DNA damage and may arise from high levels of metabolic activity. To potentially counter genomic instability caused by DNA damage, we find that hESC employ two strategies: First, these cells have enhanced levels of DNA repair proteins, including those involved in repair of DSBs, and they demonstrate elevated nonhomologous end-joining (NHEJ) activity and repair efficacy, one of the main pathways for repairing DSBs. Second, they are hypersensitive to DNA damaging agents, as evidenced by a high level of apoptosis upon irradiation. Importantly, iPSC, unlike the parent cells they are derived from, mimic hESC in their ROS levels, cell cycle profiles, repair protein expression and NHEJ repair efficacy, indicating reprogramming of the DNA repair pathways. Human iPSC however show a partial apoptotic response to irradiation, compared to hESC. We suggest that DNA damage responses may constitute important markers for the efficacy of iPSC reprogramming.

Keywords

DNA damage; DNA double strand break repair; Nonhomologous end-joining; Induced pluripotent stem cells; Human embryonic stem cells

[*]Corresponding author. Tel.: +1 410 706 5337; fax: +1 410 706 6666. frassool@som.umaryland.edu (F.V. Rassool).
[1]These authors contributed equally to the work.

Conflict of interest statement
The authors indicate no potential conflict of interest.

Appendix A. Supplementary data
Supplementary data associated with this article can be found, in the online version, at doi:10.1016/j.mrfmmm.2011.05.018.

1. Introduction

Somatic cells have functions and requirements that are very different from those of germ cells or embryonic stem cells (ESC). For example, somatic cells have restricted patterns of gene expression that are characteristic of their specific differentiated lineage, while ESC are pluripotent and possess a characteristic gene expression profile [1,2]. Embryonic SC give rise to all the cells in an organism and retain this potential, whereas differentiated cells have a limited and defined lifespan. Adult somatic cells can be induced to “dedifferentiate” into induced pluripotent stem cells (iPSC) and reprogram into cells of all three germ layers [3]. Recent advances in iPSC research have significantly changed our perspective for regenerative medicine. Patient-specific iPSC have been derived not only for disease modeling but also as sources for cell replacement therapy [3]. However, there have been insufficient data to prove that iPSC are functionally equivalent to human ESC (hESC) or are safer than hESC [4].

One area of investigation that has been little pursued is comparing how hESC and iPSC protect genomic integrity, and, thus, the integrity of the organism. Human ESC have evolved multiple mechanisms to protect their genome from various types of DNA damage. The vast majority of studies addressing this issue have been performed in mouse ESC (mESC), and while it is expected that hESC should demonstrate similar characteristics, many of these studies are yet to be performed. One key characteristic of mESC, although the precise mechanisms are not clear, is that they display substantially lower mutation frequencies than differentiated counterparts. For example, for a selectable introduced reporter gene APRT, or HPRT, mESC generate lower mutation frequencies than somatic cell counterparts [5,6]. Mouse ESC also appear to be exquisitely sensitive to DNA damage and readily undergo apoptosis or differentiation which will remove these cells from the gene pool of the organism [7-9]. Furthermore, mESC fail to arrest in G1 after DNA damage, and can then transit into S phase where they may be subject to mitotic catastrophe and thus cell death [10,11].

In considering the above protective responses, it is essential to determine more precisely the molecular mechanisms underlying how hESC protect against transmitting consequences of faulty repair of double strand breaks (DSBs) to more differentiated cells and compare how these parameters function in iPSC. In this regard, DSBs are the most lethal form of DNA damage and non-repair, or incorrect repair, can have disastrous consequences including cell death, genomic instability and cancer. The cytotoxicity of DSBs presumably reflects the difficulty of repairing these lesions because, unlike almost all other types of DNA damage that can employ an intact undamaged template strand to guide the repair, the integrity of both strands of the duplex is lost. Thus, cells that incur more than one DSB have the problem of distinguishing between the previously linked DNA ends and DNA ends from other molecules.

There are at least two pathways by which DSBs can be repaired. Homologous recombination (HR) repair performs error-free repair by utilizing the undamaged sister chromatid as the template for repair [12,13]. The nonhomologous end-joining (NHEJ) pathway joins DNA ends directly in a reaction that is independent of extensive DNA sequence homology, and is therefore prone to introducing errors during the processing and joining of non-compatible DNA ends [12-14]. Repair of DSBs by this pathway results in the addition or loss of few nucleotides at the break site. There is, however, increasing evidence for an alternative version of NHEJ (Alt NHEJ) that results in larger deletions and chromosomal translocations [15,16]. This repair is active at very low levels in normal cells [17]. The hallmark features of the Alt NHEJ pathway are that the repair junctions are characterized by larger DNA deletions, insertions, and tracts of microhomology [15].

Considering the need for high fidelity repair in ESC, it would stand to reason that HR would primarily be used to repair DSBs. Several lines of circumstantial evidence suggest that this is the case although functional analysis of HR in mESC is lacking. Mouse ESC spend about 75% of their time in S-phase the phase in which HR is active [11]. Interestingly, there appear to be no differences in expression of C-NHEJ protein XRCCIV between mouse embryonic fibroblasts (MEF) and mESC, suggesting that NHEJ may also be important in repair of DSBs in ESC [18]. There are limited studies that compare DSB repair capacity between hESC and differentiated cells. Using repair of DSBs initiated by the ISCE-1 endonuclease, while NHEJ occurs frequently in differentiated wild-type cells, mESC mainly repair DSBs by HR with a small proportion repaired by NHEJ [19]. In contrast, using the RAG system important in the generation of immunoglobulin gene rearrangements, the majority of DSBs were repaired by NHEJ [20]. These results are not paradoxical, since clearance of the RAG post-cleavage complex requires the function of specific NHEJ factors (e.g. Artemis), which is not relevant for NHEJ of other breaks. Nevertheless, more recent studies suggest that ESC use both HR and NHEJ to repair DSBs, and that both repair pathways perform efficacious repair in these cells. Adams et al., characterized the quality of DSB repair in hESC, and *in vitro*-derived neural cells. The resolution of RAD51 foci, indicative of active HR, showed that hESC as well as neural progenitors (NPs) have high capacity for HR, whereas astrocytes do not [21]. The same group later showed that while NHEJ kinetics were several-fold slower in hESC and NPs than in astrocytes derived from hESC, it is largely independent of ATM, DNA-PKcs, and PARP but dependent on XRCC4 with repair fidelity several-fold greater than in astrocytes [22].

We now, in an effort to learn more about how hESC and iPSC protect genomic integrity against potentially lethal DSBs, compare these cells for the proteins active in both HR and NHEJ pathways. We find both pathways are highly active. Moreover, while NHEJ is potentially error-prone, repair of DSBs in hESC appears to have high repair efficacy. Embryonic SC also protect the genome by having a low apoptotic threshold in response to DNA damage. Human iPSC, as compared to their parent cells of origin and ESC, do appear to completely reconstitute the above pattern of proteins for NHEJ response but demonstrate a partial apoptotic response. Our present findings suggest that monitoring of DNA repair responses may constitute one means for examining completeness of iPSC reprogramming and for considering future use of these cells in regenerative medicine

2. Materials and methods

2.1. Cell culture

Human mesenchymal stem cells (hMSC) were isolated from bone marrow obtained from the Specimen Accessioning Core at Johns Hopkins, and cultured in low glucose Dulbecco's Modified Earle's Medium (DMEM, Invitrogen, Carlsbed, CA) containing 10% FBS (Hyclone, Thermo scientific, Waltham, MA) and 1 ng/ml basic fibroblast growth factor (bFGF, BD Biosciences, Franklin Lakes, NJ). Primary human liver fibroblasts (LC2) were obtained from Coriell (New Jersey) and cultured in Eagle's Minimum Essential Medium (EMEM) with Earle's salts and non-essential amino acids (NEAA, Invitrogen) supplemented with 2 mM glutamine and 15% FBS (Sigma–Aldrich, Saint-Louis, MO). Humans ESC (WA09 or H9 and WA01 or H1, WiCell, Madison, WI) and iPSC (iMSC and iLC2) were cultured on irradiated MEF feeder layers in knockout DMEM supplemented with 20% knockout serum reconstitute (KOSR), NEAA, 0.1 mM β-mercaptoethanol, GlutaMAX and 10 ng/ml bFGF. Before performing immunostaining of FACS analysis, hESC and iPSC were transitioned on pre-coated plates with BD Matrigel™ Matrix (BD Biosciences) in MEF conditioned media. This study was done in accordance with Johns Hopkins ISCRO regulations and following a protocol approved by the Johns Hopkins IRB.

2.2. Generation of iPSC and staining for stem cell markers

2.2.1. Retroviral production and reprogramming of MSC and fibroblasts—

Retroviruses for the four factors were independently produced after co-transfecting the 293T cell line with pMX retroviral vectors expressing Oct4, Sox2, Klf4 or c-Myc (Addgene, Cambridge, MA) and helper plasmids as we previously described for reprogramming human hepatocytes and hMSC [23]. A 1:1:1:1 mix of retroviruses containing Oct4, Sox2, Klf4 and c-Myc was added to human fibroblasts (passage 3) in the presence of 8 μg/ml polybrene. Media was replaced with hESC medium at day 3. After transformed colonies were observed in the reprogramming plates, a pluripotent stem cell marker, TRA-1-60 antibody (1:200, Millipore, Billerica, MA) and Alexa 555 conjugated anti-mouse IgM antibody (1:500, Invitrogen) were added into live cell culture and incubated for 1 h at 37 °C, to distinguish the iPSC from non-iPSC colonies. TRA-1-60 positive colonies started to appear in about 6–10 days after retroviral transduction, and individual TRA-1-60 positive colonies were picked onto MEF coated plates at day 13.

2.2.2. Immunofluorescence and FACS analysis—

Cells were fixed with 4% paraformaldehyde. The following antibodies were used: TRA-1-60 (1:100, Millipore); SSEA-4 (1:200, Cell Signaling, Danvers, MA), SSEA-3 (1:200, Millipore); Tuj1 (1:500, Covance, Gaithersburg, MD), α-fetoprotein (AFP, 1:200, Dako, Carpinteria, CA), smooth muscle β-actin (SMA, 1:100, Dako), OCT4 (1:100, Millipore), NANOG (1:200, BD biosciences), anti-SSEA-3 488 from eBio-sciences, San Diego, CA. Secondary antibodies used were all of the Alexa Fluor Series from Invitrogen.

2.2.3. Embryoid body formation and spontaneous differentiation into three germ layer cells—

Human iPSC were dissociated by collagenase IV digestion and plated in ultra low attachment plates (Corning, Lowell, MA) at the density of ~1×10^6 cells/well in the presence of differentiation medium (DMEM supplemented with 20% FBS, ι-glutamine, β-mercaptoethanol, and NEAA). 50% of the medium was replaced with fresh medium every 2 days. After 7 days the embryoid bodies (EBs) were transferred to 0.1% gelatin-coated culture dishes and cultured for additional 3 days before fixation and staining. Antibodies against Tuj1 (1:500, Covance), AFP (1:200, Dako), or SMA (1:100, Dako) were used to detect the spontaneously differentiated cells from EBs.

2.2.4. Teratoma formation—

Ten-week-old male NOD/SCID/Il2γC−/− mice (Jackson ImmunoResearch Laboratories, West Grove, PA) were anesthetized and ~1 million iLC cells, resuspended in 20–40 μl of 50% matrigel, were injected subcutaneously. Mice were euthanized 12 weeks after cell injection and tumors were analyzed following H&E protocol. All animal experiments were conducted following experimental protocols previously approved by Johns Hopkins IACUC.

2.3. Measurement of intracellular reactive oxygen species (ROS) levels

Intracellular ROS levels were determined by staining with the probe 2′,7′-dichlorodihydro-fluorescein diacetate (H2DCFDA, Invitrogen). H2DCFDA was dissolved in 100% ethanol and added to the cell suspension to a final concentration of 10 μM, followed by incubation at 37 °C for 20 min. The cell pellet was resuspended in 500 μL of PBS. ROS level in cells was determined by flow cytometry (BD Biosciences, FACScan).

2.4. Immunofluorescence staining for DNA repair proteins

Human ESC and iPS cells were grown on Lab-Tek permanox chamber slide coated with BD Matrigel™ Matrix according to the instructions of the manufacturer and MSC and LC2 on Lab-TekII glass chamber slide (Lab-Tek, Thermo Scientific). Cells were then irradiated or

not at room temperature as described on the figure using Pantak HF320 X-Ray machine (250 kV peak, 13 mA; half-value layer, 1.65 mm copper) at a dose rate of 2.4 Gy/min. At the indicated time described on the figures, cells were fixed in 4% paraformaldehyde (Sigma–Aldrich) for 10 min at room temperature, permeabilized for 5 min in permeabilization solution (50 mM NaCl, 3 mM $MgCl_2$, 10 mM HEPES, 200 mM sucrose and 0.5% Triton X-100 in PBS 1×) and then blocked for an hour to overnight in DPBS + 1%BSA supplemented with 10% FBS. After washing (0.1% Triton X-100, DPBS, 5 min × 3 on a shaker), slides were incubated for 1 h with mouse anti-γH2AX antibody (1:100, Millipore) and co-immunostained with goat anti-Ku70 antibody (1:100, C-19) or rabbit RAD51 (1:100, Santa Cruz biotechnologies, Santa Cruz, CA) at 37 °C. After washing (as above), slides were incubated with secondary antibodies DyLight 594 anti-mouse and DyLight 488 anti-goat or anti-rabbit (1:200; KPL, Gaithersburg, MD) for 1 h. This series of fluorochromes consistently gives stronger and more stable fluorescent signals. Slides were washed (as above) and dried prior to counterstaining with 4′,6-diamidino-2-phenylindole (DAPI; Vector Laboratories, Burlingame, CA). Slides were examined using a Nikon fluorescent microscope Eclipse 80i (100×/1.4 oil, Melville, NY) and images of at least 50 cells/slide were captured using a CCD (charge-coupled device) camera and the imaging software NIS Elements (BR 3.00, Nikon).

2.5. Cell cycle profile

Cells were harvested with trypsin/EDTA 0.05% and 0.5×10^6 cells were washed in PBS-FBS2% in order to obtain a single cell suspension. Cells were then fixed in EtOH 70% for 1 h at 4 °C, wash twice in PBS-FBS2% and stained for 45 min in the dark in 0.05 mg/ml propidium iodide (PI), 1 mg/ml RNase A, 0.3% Triton X-100. Cell cycle profile was analyzed in FlowJo software using Watson pragmatic model (BD Biosciences, FACScan)

2.6. Whole cell extracts, immunoblotting and in vitro NHEJ

2.6.1. Whole cell extracts (WCE)—Whole cell extracts were prepared according to Buck et al. [24]. Cells were suspended in lysis buffer (25 mM Tris–HCl pH 7.5, 333 mM KCl, 1.3 mM EDTA, 4 mM DTT, protease inhibitor cocktail (Roche, Branchburg, NJ) and phosphatase inhibitors cocktail (Sigma–Aldrich). The cell suspension was subject to 3 cycles of snap freezing and thaw at 30 °C. The lysates were incubated on ice for 30 min and cleared by centrifugation (16,000 × *g*, 15 min) at 4 °C. The supernatants were transferred to a 1 kDa cut-off mini dialysis tube (GE Healthcare, Piscataway, NJ) and dialyzed twice for an hour against buffer E (20 mM Tris–HCl pH 8.0, 20% glycerol, 0.1 M K(OAc), 0.5 mM EDTA, 1 mM DTT).

2.6.2. Immunoblotting—Proteins concentrations in WCE were quantified using Bradford reagents (Sigma–Aldrich) and 20 μg of proteins were separated by electrophoresis through either 4–7% or 4–10% SDS-polyacrylamide gradient gels and then transferred to PVDF membranes. After blocking, membranes were probed with primary antibodies Rabbit Rad51, goat Ku70 (1:1000, C-19, Santa Cruz), XLF (1:1000, Cell Signaling), PARP1 (1:10,000, Ebiosciences), XRCCI (1:2000, Genetex, Irvine, CA), XRCCIV (1:500, Santa Cruz), DNA Ligase IIIα (DNA LigIIIα, 1:500, Genetex), DNA LigIV (1:500, Santa Cruz) and β-actin as a loading control (1:5000, Sigma–Aldrich). After probing with adequate secondary antibodies (Jackson ImmunoResearch Laboratories), proteins expression was detected using enhanced chemiluminescence (ECL; 100 mM Tris–HCl pH 8.5, luminal, coumaric acid, and hydrogen peroxide).

2.6.3. In Vitro NHEJ assay—*In vitro* NHEJ assay were performed using a procedure adapted from Baumann et al. and Buck et al. [24]. Briefly, WCE were adjusted to 5 μg/μl and 20 μg of WCE were incubated in 10 μl reaction with 50 ng of linear DNA (pUC19

digested with BAMHI (Compatible end, ThermoFisher Scientific)) or pAcGFP1-N2 digested with SacI and KpnI (Uncompatible end, Clontech, Mountain View, CA) in 5× ligation buffer (250 mM Tris–HCl pH 7.5, 250 mM KCl, 0.5 mg/ml BSA, 25 mM ATP, 25 mM $MgCl_2$, 5 mM DTT, 5% glycerol, 25 μM dNTPs mix, proteinase inhibitor cocktail) for 2 h at 25 °C. Reactions were then treated with 1 μl RNase (1 mg/ml) for 5 min at room temperature and with 2 μl of 5× deproteination solution (10 mg/ml Proteinase K, 2.5% SDS, 50 mM EDTA, 100 mM Tris–HCl pH 7.5) for 30 min at 55 °C. DNA in the supernatant was co-precipitated with Pellet pain (Invitrogen). After migration of the samples in 0.7% agarose, the gels were stained with SYBR-Green (30 min, Invitrogen), and fluorescence was detected via a FluorImager (Bio-Rad, Hercules, CA). Ligated plasmid was calculated relative to total DNA loaded and expressed as relative ligation efficiency.

For DNA sequencing of DSB repair junctions, PCR was performed using the purified ligated pACGFP-N2 DNA as template. The primers (forward TGCCCACTTGGCAGTACATCAA; reverse ATGGCGCTCTTGAAGAAGTCGT) were designed to amplify a 738 bp fragment from the intact pAcGFP1-N2 across the SacI and KpnI cutting sites. The PCR products were purified using MinElute PCR purification kit (Qiagen, Valencia, CA), and cloned into TOPO TA cloning vectors (Invitrogen). DNA was sequenced in our core sequencing facility and analyzed. The Blast program from the NCBI web site was used for sequence alignment.

3. Results

3.1. Characterization of hiPSC

To initially characterize DNA damage responses in hESC vs iPSC, and how these latter cells may reprogram these parameters, we examined induced liver pluripotent cells (iLC2) and induced mesenchymal stem cells (iMSC), iPSC derived from liver fibroblast cells (LC2) and mesenchymal stem cells (MSC), respectively. iMSC were previously described and iLC2 were newly derived, by retroviral transduction of LC2 with Oct4, Sox2, Klf4 and c-Myc, as described in Section 2 [23,25-27]. Both iLC2 and iMSC demonstrate classical iPSC features, including their morphology in culture, TRA-1-60 staining, and cystic teratoma formation with three germ layer derivatives (Figure S1A–D) [25]. Induced LC2 and iMSC expressed endogenous transcriptional regulators and cell-surface markers characteristic of hESC, including NANOG, OCT4, SSEA-4, and TRA-1-60 (Figure S1A) [25]. Overall, the expression of stem cell markers in iLC2 was indistinguishable from hESC we examined, H1 and H9, maintained under the same conditions [23]. These lines have been maintained in continuous culture for over 10 months without signs of replicative or karyotypic crisis (Figure S1B).

3.2. Comparison of ROS levels, endogenous DNA damage and cell cycle profile between hESC, iPSC and parental control

Levels of ROS are tightly regulated in cells [28] and excessive levels can lead to oxidative DNA adducts and actual DNA strand breakage, that includes both SSBs and DSBs [29]. Using a previously described flow cytometric measurement of ROS [30,31], we found no significant differences in ROS levels between hESC lines (H1 and H9) and the iPSC (iMSC and iLC2) (Fig. 1A) but both have a significant (>2-fold) increase in ROS, compared with parental MSC and LC2 cells (H1 vs LC2, $p = 0.032$; H9 vs LC2, $p = 0.037$; iMSC vs MSC, $p = 0.018$; iLC2 vs LC2, $p = 0.022$; Fig. 1A).

To investigate whether increased levels of ROS translate into increased levels of DNA damage, we next measured γH2AX foci, established markers for DSBs, using previously described immunostaining techniques [17,32]. H1 and H9 cells exhibit a very low mean

number of foci per cell, compared with primary fibroblasts LC2 (H1 vs LC2, $p = 0.003$; H9 vs LC2, $p = 0.002$) and MSC (H1 vs MSC, $p = 0.002$; H9 vs MSC, $p = 0.001$) (Fig. 1B and C). Importantly, iPSC derived from MSC exhibit a very low mean γH2AX foci per cell similar to hESC and significantly different from the parental cells from which they were derived (iMSC vs MSC, $p = 0.001$; iLC2 vs LC2, $p = 0.002$) (Fig. 1B and C).

It is well established that the cell cycle profiles in embryonic cells are different from those of differentiated cells [10,11]. For example, a larger proportion of ESC appear to be in S phase and this could aid cells in combating genomic instability, whereby cells with excessive DNA damage may be subject to mitotic catastrophe and thus cell death [10,11]. We thus analyzed the cell cycle profile of the six different cell lines using propidium iodide staining (Fig. 1D and E). Our results show that hESC (H1 and H9) and iPSC (iMSC and iLC2) exhibit a similar pattern of highly proliferative cells with 48–55% of the cells in S phase, 15–31% in G2, 17–34% in G1. In contrast, parental control cells, MSC and LC2, exhibit a pattern of differentiated cells with 30–37% of the cells in S phase, 3–12% in G2 and 51–68% in G1 (Fig. 1D and E). We next examined the different cell types in greater detail for similarities and differences in S and G0/G1 phases of the cell cycle. The percentage of cells in S phase in hESC and iPSC are significantly different compared to that of parental cells, MSC and LC2 (H1 vs LC2, $p = 0.0001$; H9 vs LC2, $p = 0.0001$, H1 vs MSC, $p = 0.002$, H9 vs MSC, $p = 0.001$, iMSC vs MSC, $p = 0.001$ and iLC2 vs LC2, $p = 0.0001$, Fig. 1E). While there are no significant differences between the percentage of cells in S phase in H1 or H9 vs iLC2, iMSC cells exhibit a small but significant increase in the number of cells in S phase, 55%, compared to hESC, H1 (48%), or H9 (52%) (H1 vs iMSC, $p = 0.013$, H9 vs iMSC, $p = 0.019$, Fig. 1E). As with S phase cells, hESC and iPSC cells in the G0/G1 phase are significantly different compared with parental cells, MSC and LC2 (H1 vs LC2, $p = 0.001$; H9 vs LC2, $p = 0.0001$, H1 vs MSC, $p = 0.0001$, H9 vs MSC, $p = 0.0001$, iMSC vs MSC, $p = 0.0001$ and iLC2 vs LC2, $p = 0.0001$, Fig. 1E). There are also no significant differences between the percentage of cells in G0/G1 phase in H9 vs iLC2. However, iMSC cells exhibit a significant decrease in G0/G1 phase cells, 17%, compared to hESC H1, 21% or H9, 34% (H1 vs iMSC, $p = 0.001$, H9 vs iMSC, $p = 0.0001$, Fig. 1E).

3.3. Comparison of DNA repair proteins expression in hESC, iPSC and parental control line

Given that increased levels of endogenous DNA damaging ROS were demonstrated in hESC and iPSC, yet these cells exhibited few DSBs, DNA repair could be very efficient and/or increased in these cells. To determine this, we began by measuring the steady state levels of proteins that participate in both HR and NHEJ pathways. Immunoblotting analysis for RAD51, a key HR protein that is responsible for strand invasion into the adjacent sister chromatid, demonstrates that hESC (H1 and H9) and iPSC (iMSC and iLC2) have similar expression levels and that these levels are significantly increased (approximately 10-fold), compared with parental MSC and LC2 (Fig. 2A).

We next looked at multiple proteins that participate in NHEJ and other repair pathways relevant to preventing ongoing damage from increased ROS. Ku70 is a key player in the DNA-PK dependent C-NHEJ pathway, binding to DSBs and initiating NHEJ repair [33]. Steady state levels of Ku70 protein appear similar in hESC (H1 and H9) and iPSC (iMSC and iLC2), but increased by 4-fold compared with iPSC parental controls (MSC and LC2) (Fig. 2B). In contrast, levels of DNA LigIV and XRCCIV proteins, that participate in the final ligation step of C-NHEJ, appear unchanged in hESC, iPSC and parental controls (Fig. 2A). Interestingly, another NHEJ factor, XLF or Cernunnos, that contributes to the joining of non-complementary DNA ends by interacting with DNA LigIV/XRCCIV stimulating the joining of mismatched DNA ends [34], appears increased (≥4-fold) in hESC and iPSC, as compared with parental control cells (Fig. 2A). In addition to creating strand breaks,

endogenous ROS creates oxidative DNA lesions that are repaired by base excision repair (BER) and SSB repair pathways [35]. DNA LigIIIα, XRCC1 and PARP1, that participate in both BER and SSB are also significantly upregulated in hESC and iPSC cells, as compared with parental controls (Fig. 2C). This suggests that repair proteins in hESC may be increased to combat the DNA damaging effects of endogenous ROS. Alternatively, DNA LigIIIα, XRCC1 and PARP1 may also participate in the little understood Alt NHEJ that is highly error-prone, and so may be implicated in genomic instability [15].

3.4. Comparison of DNA repair efficiency and type of repair in hESC, iPSC and parental control

We, thus, next explored in more detail, NHEJ repair in hESC, iPSC and parental controls cells. We used a plasmid-based repair assay in which linearized plasmid (50 ng), digested with restriction endonucleases resulting in compatible [Bam HI] and non-compatible [SacI/KpnI] DNA ends [24]) was incubated with 20 μg WCE prepared from hESC (H9), iPSC (iMSC) and parental MSC (Fig. 3A). Recovered DNA was then resolved on an agarose gel and NHEJ efficiency was calculated by 2D densitometry [24]. H9 cells exhibit the highest NHEJ efficiency, followed by iMSC, and the lowest end-joining efficiency was found for parental MSC (Fig. 3Bi and ii, C). While NHEJ efficiency is increased in hESC (H9) and iPSC (iMSC), compared with MSC controls, NHEJ capacity is clearly increased in hESC compared with iPSC. End-joining appears decreased in all cells tested in repair of incompatible DNA ends (Fig. 3Bii). As protein loading control, immunoblotting for β-actin from the same WCE used to performed *in vitro* NHEJ are shown and quantified (Fig. 3Biii).

Repair of DSBs by the DNA-PK dependent C-NHEJ pathway can result in the addition or loss of few nucleotides at the break site, whereas Alt NHEJ results in large DNA deletions (>20 bp) with repair occurring at regions of DNA sequence microhomology [33]. To determine how efficacious NHEJ repair in hESC is and how well iPSC reprogram the NHEJ repair response, we sequenced the repair junctions of 19–23 individuals repaired DSBs from plasmid end-joining experiments using non-compatible DNA ends and nuclear extracts from H9, iMSC and MSC cells. In C-NHEJ, single strand overhangs are generally resected and the DSBs are ligated together with or without DNA end processing, resulting in the loss of a few nucleotides. Despite the differences in NHEJ efficiency in hESC vs iPSC noted above (Fig. 3B and C), the repair junctions in plasmids recovered from H9 and iMSC were relatively accurate (91.3% and 89.47%, respectively, Fig. 4A and B) with loss of a few nucleotides at the breakpoint junction (Fig. 4C). In striking contrast, in plasmids recovered from MSC, the junctions were significantly less accurate (34.78%; Fig. 4A and B) with deletion of more than 20 nucleotides in many of the repair junctions sequenced (Fig. 4C). Finally, we examined nucleotide sequences at the breakpoint junctions from above *in vitro* DNA repair experiments, to determine whether regions of microhomology (defined as ≥2 bp) were used in repair of DSBs. We find no microhomologies in 23 DSB repair junctions analyzed from plasmids repaired by hESC H9 cell extracts, whereas using cell extracts from iMSC, 2 of 19 plasmids contained microhomologies at the repair junctions. In contrast, 8 of 23 plasmids analyzed from repair experiments involving parental MSC demonstrated microhomologies at the breakpoint junctions (Fig. 4A). In all of the DSB repair junctions analyzed, microhomologies of no more than 2 nucleotides were observed.

3.5. Comparison of DNA damage sensitivity of hESC and iPSC

To determine how hESC and iPSC cells respond to exogenous DNA damaging agents, H9 and iMSC were treated with γ irradiation and then nuclei were examined for γH2AX foci, as we previously described [17,32]. Following radiation (1 Gy, 0, 20 min, 2, 4 h), both H9 and iMSC demonstrate increased γH2AX foci with time after irradiation (Table 1). However, it appears that by 4 h after irradiation H9 cells show a general decrease in the number of foci

per cell, while in iMSC the foci appear to increase even further (Table 1). Importantly, to determine whether DSB repair proteins are recruited to γH2AX foci, H9 and iMSC were co-immunostained for NHEJ protein Ku70 and HR protein RAD51 following irradiation (1 Gy, 0, 20 min, 2, 4 h). Ku70 and Rad51 co-localize with a proportion of γH2AX foci, confirming that both repair pathways are involved in repair of DSBs in hESC and iPSC. Interestingly, there generally appear to be more Ku70 foci colocalizing with γH2AX following irradiation, compared with Rad51 (Table 1). While we observe robust foci and colocalization at higher doses, e.g. 5 Gy, 4 h (Fig. 5A and B), a significant proportion of hESC and iMSC appear to be dead or dying, making quantification of bone fide DNA damage vs apoptosis-related DNA damage difficult at these timepoints (data not shown).

3.6. Comparison of apoptotic response to DNA damage in hESC, iPSC and parental control cell line

One mechanism for hESC and iPSC to avoid transmitting ongoing genomic instability induced by DNA damage to committed progeny is to activate cell death pathways. We therefore determined whether these cells exhibit differential apoptosis in response to irradiation, compared with parental control cells. Interestingly, using Annexin V staining as an assay after cell irradiation (5 Gy, 4 h), H9 (Fig. 6A) exhibited more apoptosis than iMSC (Fig. 6B), but both of these stem cell types demonstrate far more cell death than MSC cells (Fig. 6C).

4. Discussion

Induced PSCs have shown remarkable similarity to naturally isolated pluripotent stem cells, such as mESC and hESC, for many key parameters. Induced PSC resemble hESC morphologically, forming flat, tight-edged and aggregated colonies [36]. Induced PSC are mitotically active, actively self-renewing, proliferating, and dividing at a rate equal to ESC [37]. Induced PSC express cell surface markers that are expressed on hESC. Induced PSC also express high telomerase activity as do hESC [38]. Finally, genome wide studies of gene expression, DNA methylation, and epigenome characteristics, reveal remarkable similarities. Nevertheless, in these latter studies, significant differences emerge and especially during early passages, iPSC can retain characteristics of the parent cells from which they were induced [39]. There are, then, concerns that still could prohibit the use of iPSC in the clinic. Many studies are still required to assess how well iPSC are truly reprogrammed [36].

In the present work, we have compared how hESC and iPSC compare in DNA damage and repair responses which are critical to their genetic integrity and to the genomic stability of the human organism. Several important observations have emerged which illustrate, again, the remarkable ability to reprogram committed human cells to an ESC-like phenotype. Our results suggest that hESC and iPSC both employ at least two strategies, to combat the effects of DNA damaging agents: First, they upregulate both the HR and NHEJ pathways for DNA repair as well as components of other repair pathways that respond to oxidative stress, such as BER and SSB. Our findings for hESC are consistent with some findings of others. Using single-cell gel electrophoresis (comet assay) Maynard et al. [40] found that hESC (BG01, I6) have more efficient repair of different types of DNA damage (generated from H_2O_2, UV-C, ionizing radiation, or psoralen) than human primary fibroblasts (WI-38, hs27). In addition, these investigators showed by microarray gene expression analysis that mRNA levels of several DNA repair genes are elevated in hESC compared with their differentiated forms (EBs) [40]. The second strategy employed by hESC and iPSC to combat transmission of genomic instability is that both cell types are highly sensitive to DNA damage and readily undergo apoptosis as described in others studies [7-9]. Another shared property we found for hESC and iPSC is high levels of ROS compared to the more committed parent cells studied. Interestingly in this regard, a quiescent and primitive population of adult hematopoietic stem

cells (AHSC) have been reported to demonstrate low levels of ROS, existing in a low-oxygenic osteoblastic niche in bone marrow, thus providing long-term protection for hematopoietic stem cells from genotoxic stress [41]. While, the reason for the high ROS levels in hESC and iPSC are not clearly understood, this may reflect the fact that these cells are mitotically active, and have a high proliferative index [11,28]. Importantly, both iPSC lines examined demonstrate high ROS levels and high proliferative index as in hESC but not observed in their parental counterparts.

The histone variant H2AX is rapidly phosphorylated at the sites of DSBs. This phosphorylated H2AX (γH2AX) is involved in the retention of repair and signaling factor complexes at sites of DNA damage [32]. We find that while hESC and iPSC demonstrate very low endogenous foci levels, the number γH2AX foci/cell increase dramatically following irradiation. Both NHEJ protein Ku70 and Rad51 appear to colocalize with a percentage of these foci, suggesting that both repair pathways function in hESC and iMSC. Moreover, recent studies support the notion that in ESC both HR and NHEJ perform efficient repair of DSBs [21,22]. Our studies show and that in hESC and iPSC, at least at steady state levels, HR protein RAD51 is increased about 10-fold, whereas NHEJ protein Ku70 is increased approximately 4-fold, compared with more differentiated cells. Fattah et al. recently demonstrated that in human cells, Ku is the critical C-NHEJ factor that regulates DSB repair pathway choice [42]. Thus, enhanced Ku protein expression in hESC and iPSC, may result in more efficacious NHEJ repair. Similar to results of Tichy and Stambrook using mESC, we find that levels of C-NHEJ proteins, DNA LigIV and XRCCIV, are unchanged in hESC, iPSC and parental iPSC [18], suggesting that NHEJ may operate in an equivalent manner in the different cell types. While the significance of the increased levels of XLF-Cernunnos, a component of the DNA LigIV/XRCCIV complex in hESC is unclear, XLF may promote increased DSB ligation activity, as has been suggested by Riballo et al. [43]. Moreover, recent studies suggest that ATM and XLF play a role in C-NHEJ repair, and combined deficiency severely impairs C-NHEJ and nearly blocks mouse lymphocyte development due to an inability to join V(D)J recombination intermediates [44]. In functional *in vitro* NHEJ assays, we show that hESC demonstrate robust NHEJ activity that is increased approximately 2-fold compared with parental MSC. While iPSC demonstrate an intermediate NHEJ repair activity with respect to hESC and parental controls, they show repair fidelity that is equivalent to hESC, with deletion of a few nucleotides and with little or no microhomology sequences occurring at the junctions of repaired DSBs. In contrast, parental MSC show an increased frequency of larger DNA deletions and use of microhomologies at the repair junctions. Interestingly, the studies of Rahal et al., showed that ATM suppresses DSB repair by microhomology-mediated end joining (MMEJ) and that Mre11 is the major nuclease behind increased DNA end-degradation and MMEJ repair in ataxia telangietasia (A-T) cells that lack ATM [45,46]. Numerous studies have shown that DNA repair factors are significantly affected by cell cycle phase [47]. In our studies, hESC and iPSC exhibit a highly proliferative cell cycle profile compared to the more differentiated profile of the parental cells. Nevertheless, iMSC exhibit a significantly higher percentage of cells in S-phase, compared with hESC. The HR pathway, which is active in late S phase and in the G2 phase of the cell cycle, utilizes the undamaged sister chromatid as the template for repair and so is usually error-free [48]. While HR repair has not been examined in this study, steady state levels of HR proteins, such as RAD51, do not appear different between hESC and iMSC cells. Notably, the percentage of cells in G0/G1 was 2-fold lower in iMSC, compared with H9 hESC. Given that NHEJ is the major DSB repair pathway in G0/G1 and early S phase [47], the decreased NHEJ repair activity we have demonstrated in iMSC may be explained by this difference.

One potentially important question in the science of iPSC, is what degree of reprogramming is necessary to functionally and efficaciously regenerate cells. Cellular apoptotic responses

are arguably one of the vital protective responses of an organism. Our studies show that while iPSC derivatives show an increased level of apoptosis compared with parental derivatives, hESC are nearly twice as sensitive to DNA damaging agents. The reason for these differences is not understood, but may reflect several factors. One could be that we have studied iPSC at relatively early passages (~passage 15–30) compared to ESC (~passage 30–40), and some ESC properties of these iPSC have been observed to increase in later passages of iPSC [39]. Thus, additional studies are still required to assess how well iPSC are truly reprogrammed and factors such as the cell of origin [49], use of non-viral technology, etc., may yield differences in the efficacy of reprogramming [36]. Our studies suggest that study of DNA damage repair responses may provide another good monitor for gauging the re-programming efficacy of iPSC prepared using multiple approaches.

5. Conclusion

The DNA damage response in ESC is critical for the maintenance of genomic integrity of the organism. Induced PSC have great potential in regenerative medicine, however, few studies have examined how well the DNA damage response is reprogrammed. We report that hESC demonstrate an enhanced DNA repair response and a low threshold for inducing apoptosis, compared with more differentiated cells. Importantly, iPSC fully reprogram the DNA repair response, but demonstrate a partial apoptotic response compared to hESC. Thus, the DNA damage and repair response may provide an additional marker in studies to determine the efficacy of reprogramming by various means.

Supplementary Material

Refer to Web version on PubMed Central for supplementary material.

Acknowledgments

This work was supported by Maryland Stem Cell Research Fund grants # 103655, 103974, 108592 and 108563.

Flow cytometry for ROS and cell cycle analysis were performed at the University of Maryland Greenbaum Cancer Center Shared Flow Cytometry Facility.

References

1. Bhattacharya B, Puri S, Puri RK. A review of gene expression profiling of human embryonic stem cell lines and their differentiated progeny. Curr Stem Cell Res Ther. 2009; 4:98–106. [PubMed: 19442194]
2. Rao RR, Stice SL. Gene expression profiling of embryonic stem cells leads to greater understanding of pluripotency and early developmental events. Biol Reprod. 2004; 71:1772–1778. [PubMed: 15140800]
3. Lengner CJ. iPS cell technology in regenerative medicine. Ann N Y Acad Sci. 2010; 1192:38–44. [PubMed: 20392216]
4. Carpenter MK, Couture LA. Regulatory considerations for the development of autologous induced pluripotent stem cell therapies. Regen Med. 2010; 5:569–579. [PubMed: 20632860]
5. Thomas JW, LaMantia C, Magnuson T. X-ray-induced mutations in mouse embryonic stem cells. Proc Natl Acad Sci U S A. 1998; 95:1114–1119. [PubMed: 9448294]
6. Munroe RJ, Bergstrom RA, Zheng QY, Libby B, Smith R, John SW, Schimenti KJ, Browning VL, Schimenti JC. Mouse mutants from chemically mutagenized embryonic stem cells. Nat Genet. 2000; 24:318–321. [PubMed: 10700192]
7. Park Y, Gerson SL. DNA repair defects in stem cell function and aging. Annu Rev Med. 2005; 56:495–508. [PubMed: 15660524]

8. Roos WP, Christmann M, Fraser ST, Kaina B. Mouse embryonic stem cells are hypersensitive to apoptosis triggered by the DNA damage O(6)-methylguanine due to high E2F1 regulated mismatch repair. Cell Death Differ. 2007; 14:1422–1432. [PubMed: 17464330]
9. Van Sloun PP, Jansen JG, Weeda G, Mullenders LH, van Zeeland AA, Lohman PH, Vrieling H. The role of nucleotide excision repair in protecting embryonic stem cells from genotoxic effects of UV-induced DNA damage. Nucleic Acids Res. 1999; 27:3276–3282. [PubMed: 10454634]
10. Aladjem MI, Spike BT, Rodewald LW, Hope TJ, Klemm M, Jaenisch R, Wahl GM. ES cells do not activate p53-dependent stress responses and undergo p53-independent apoptosis in response to DNA damage. Curr Biol. 1998; 8:145–155. [PubMed: 9443911]
11. Savatier P, Lapillonne H, Jirmanova L, Vitelli L, Samarut J. Analysis of the cell cycle in mouse embryonic stem cells. Methods Mol Biol. 2002; 185:27–33. [PubMed: 11768996]
12. Khanna KK, Jackson SP. DNA double-strand breaks: signaling, repair and the cancer connection. Nat Genet. 2001; 27:247–254. [PubMed: 11242102]
13. Hartlerode AJ, Scully R. Mechanisms of double-strand break repair in somatic mammalian cells. Biochem J. 2009; 423:157–168. [PubMed: 19772495]
14. Lieber MR. The mechanism of human nonhomologous DNA end joining. J Biol Chem. 2008; 283:1–5. [PubMed: 17999957]
15. Nussenzweig A, Nussenzweig MC. A backup DNA repair pathway moves to the forefront. Cell. 2007; 131:223–225. [PubMed: 17956720]
16. Iliakis G. Backup pathways of NHEJ in cells of higher eukaryotes: cell cycle dependence. Radiother Oncol. 2009; 92:310–315. [PubMed: 19604590]
17. Sallmyr A, Tomkinson AE, Rassool FV. Up-regulation of WRN and DNA ligase IIIalpha in chronic myeloid leukemia: consequences for the repair of DNA double-strand breaks. Blood. 2008; 112:1413–1423. [PubMed: 18524993]
18. Tichy ED, Stambrook PJ. DNA repair in murine embryonic stem cells and differentiated cells. Exp Cell Res. 2008; 314:1929–1936. [PubMed: 18374918]
19. Francis R, Richardson C. Multipotent hematopoietic cells susceptible to alternative double-strand break repair pathways that promote genome rearrangements. Genes Dev. 2007; 21:1064–1074. [PubMed: 17473170]
20. Cui X, Meek K. Linking double-stranded DNA breaks to the recombination activating gene complex directs repair to the nonhomologous end-joining pathway. Proc Natl Acad Sci U S A. 2007; 104:17046–17051. [PubMed: 17939999]
21. Adams BR, Golding SE, Rao RR, Valerie K. Dynamic dependence on ATR and ATM for double-strand break repair in human embryonic stem cells and neural descendants. PLoS One. 2010; 5:e10001. [PubMed: 20368801]
22. Adams BR, Hawkins AJ, Povirk LF, Valerie K. ATM-independent, high-fidelity nonhomologous end joining predominates in human embryonic stem cells. Aging (Albany NY). 2010; 2:582–596. [PubMed: 20844317]
23. Liu H, Ye Z, Kim Y, Sharkis S, Jang YY. Generation of endoderm-derived human induced pluripotent stem cells from primary hepatocytes. Hepatology. 2010; 51:1810–1819. [PubMed: 20432258]
24. Buck D, Malivert L, de Chasseval R, Barraud A, Fondaneche MC, Sanal O, Plebani A, Stephan JL, Hufnagel M, le Deist F, Fischer A, Durandy A, de Villartay JP, Revy P. Cernunnos, a novel nonhomologous end-joining factor, is mutated in human immunodeficiency with microcephaly. Cell. 2006; 124:287–299. [PubMed: 16439204]
25. Liu H, Kim Y, Sharkis S, Ye Z, Jang YY. Hepatic differentiation from virus-free and integration-free human induced pluripotent stem cells. Hepatology. 2010; 52:1169–1170. [PubMed: 20812362]
26. Ye Z, Zhan H, Mali P, Dowey S, Williams DM, Jang YY, Dang CV, Spivak JL, Moliterno AR, Cheng L. Human-induced pluripotent stem cells from blood cells of healthy donors and patients with acquired blood disorders. Blood. 2009; 114:5473–5480. [PubMed: 19797525]
27. Liu H, Kim Y, Sharkis S, Marchionni L, Jang YY. In vivo Liver Regeneration Potential of Human Induced Pluripotent Stem Cells from Diverse Origins. Sci Transl Med. 2011; 3:82ra39.

28. Vallyathan V, Shi X. The role of oxygen free radicals in occupational and environmental lung diseases. Environ Health Perspect. 1997; 105(Suppl. 1):165–177. [PubMed: 9114285]
29. Karanjawala ZE, Murphy N, Hinton DR, Hsieh CL, Lieber MR. Oxygen metabolism causes chromosome breaks and is associated with the neuronal apoptosis observed in DNA double-strand break repair mutants. Curr Biol. 2002; 12:397–402. [PubMed: 11882291]
30. Rassool FV, Gaymes TJ, Omidvar N, Brady N, Beurlet S, Pla M, Reboul M, Lea N, Chomienne C, Thomas NS, Mufti GJ, Padua RA. Reactive oxygen species, DNA damage, and error-prone repair: a model for genomic instability with progression in myeloid leukemia? Cancer Res. 2007; 67:8762–8771. [PubMed: 17875717]
31. Sallmyr A, Fan J, Rassool FV. Genomic instability in myeloid malignancies: increased reactive oxygen species (ROS), DNA double strand breaks (DSBs) and error-prone repair. Cancer Lett. 2008; 270:1–9. [PubMed: 18467025]
32. Lobrich M, Shibata A, Beucher A, Fisher A, Ensminger M, Goodarzi AA, Barton O, Jeggo PA. gammaH2AX foci analysis for monitoring DNA double-strand break repair: strengths, limitations and optimization. Cell Cycle. 2010; 9:662–669. [PubMed: 20139725]
33. Rassool FV, Tomkinson AE. Targeting abnormal DNA double strand break repair in cancer. Cell Mol Life Sci. 2010; 67:3699–3710. [PubMed: 20697770]
34. Ahnesorg P, Smith P, Jackson SP. XLF interacts with the XRCC4-DNA ligase IV complex to promote DNA nonhomologous end-joining. Cell. 2006; 124:301–313. [PubMed: 16439205]
35. Adhikari S, Choudhury S, Mitra PS, Dubash JJ, Sajankila SP, Roy R. Targeting base excision repair for chemosensitization. Anticancer Agents Med Chem. 2008; 8:351–357. [PubMed: 18473720]
36. Yamanaka S, Blau HM. Nuclear reprogramming to a pluripotent state by three approaches. Nature. 2010; 465:704–712. [PubMed: 20535199]
37. Ghule PN, Medina R, Lengner CJ, Mandeville M, Qiao M, Dominski Z, Lian JB, Stein JL, van Wijnen AJ, Stein GS. Reprogramming the pluripotent cell cycle: restoration of an abbreviated G1 phase in human induced pluripotent stem (iPS) cells. J Cell Physiol. 2011; 226:1149–1156. [PubMed: 20945438]
38. Kim EY, Jeon K, Park HY, Han YJ, Yang BC, Park SB, Chung HM, Park SP. Differences between cellular and molecular profiles of induced pluripotent stem cells generated from mouse embryonic fibroblasts. Cell Reprogram. 2010; 12:627–639. [PubMed: 20958217]
39. Kim K, Doi A, Wen B, Ng K, Zhao R, Cahan P, Kim J, Aryee MJ, Ji H, Ehrlich LI, Yabuuchi A, Takeuchi A, Cunniff KC, Hongguang H, McKinney-Freeman S, Naveiras O, Yoon TJ, Irizarry RA, Jung N, Seita J, Hanna J, Murakami P, Jaenisch R, Weissleder R, Orkin SH, Weissman IL, Feinberg AP, Daley GQ. Epigenetic memory in induced pluripotent stem cells. Nature. 2010; 467:285–290. [PubMed: 20644535]
40. Maynard S, Swistowska AM, Lee JW, Liu Y, Liu ST, Da Cruz AB, Rao M, de Souza-Pinto NC, Zeng X, Bohr VA. Human embryonic stem cells have enhanced repair of multiple forms of DNA damage. Stem Cells. 2008; 26:2266–2274. [PubMed: 18566332]
41. Jang YY, Sharkis SJ. A low level of reactive oxygen species selects for primitive hematopoietic stem cells that may reside in the low-oxygenic niche. Blood. 2007; 110:3056–3063. [PubMed: 17595331]
42. Fattah F, Lee EH, Weisensel N, Wang Y, Lichter N, Hendrickson EA. Ku regulates the non-homologous end joining pathway choice of DNA double-strand break repair in human somatic cells. PLoS Genet. 2010; 6:e1000855. [PubMed: 20195511]
43. Riballo E, Woodbine L, Stiff T, Walker SA, Goodarzi AA, Jeggo PA. XLF-Cernunnos promotes DNA ligase IV-XRCC4 re-adenylation following ligation. Nucleic Acids Res. 2009; 37:482–492. [PubMed: 19056826]
44. Zha S, Guo C, Boboila C, Oksenych V, Cheng HL, Zhang Y, Wesemann DR, Yuen G, Patel H, Goff PH, Dubois RL, Alt FW. ATM damage response and XLF repair factor are functionally redundant in joining DNA breaks. Nature. 2011; 469:250–254. [PubMed: 21160472]
45. Rahal EA, Henricksen LA, Li Y, Williams RS, Tainer JA, Dixon K. ATM regulates Mre11-dependent DNA end-degradation and microhomology-mediated end joining. Cell Cycle. 2010; 9:2866–2877. [PubMed: 20647759]

46. Rahal EA, Henricksen LA, Li Y, Turchi JJ, Pawelczak KS, Dixon K. ATM mediates repression of DNA end-degradation in an ATP-dependent manner. DNA Repair (Amst). 2008; 7:464–475. [PubMed: 18207464]

47. Lieber MR. The mechanism of double-strand DNA break repair by the nonhomologous DNA end-joining pathway. Annu Rev Biochem. 2010; 79:181–211. [PubMed: 20192759]

48. Takata M, Sasaki MS, Sonoda E, Morrison C, Hashimoto M, Utsumi H, Yamaguchi-Iwai Y, Shinohara A, Takeda S. Homologous recombination and nonhomologous end-joining pathways of DNA double-strand break repair have overlapping roles in the maintenance of chromosomal integrity in vertebrate cells. EMBO J. 1998; 17:5497–5508. [PubMed: 9736627]

49. Broxmeyer HE. Will iPS cells enhance therapeutic applicability of cord blood cells and banking? Cell Stem Cell. 2010; 6:21–24. [PubMed: 20074533]

Abbreviations

AHSC	adult hematopoietic stem cells
DSB	double strand break
ESC	embryonic stem cells
HR	homologous recombination
iPSC	induced pluripotent stem cells
MMEJ	microhomology mediated end joining
MSC	mesenchymal stem cells
NHEJ	nonhomologous end joining
NP	neural progenitor
ROS	reactive oxygen species

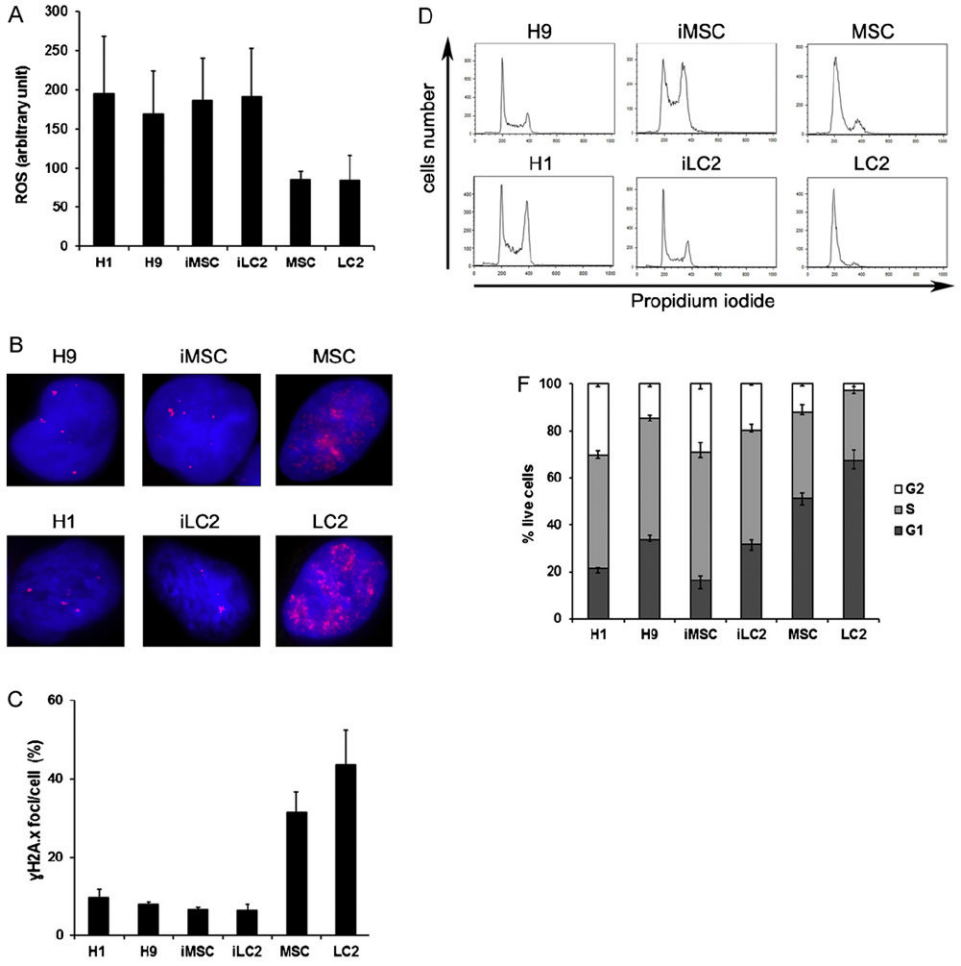

Fig. 1.

ROS levels, γH2AX expression and cell cycle profile in hESC, iPSC and parental control cells. (A) Endogenous ROS was measured by staining hESC (H1 and H9), iPSC (iMSC and iLC2), and parental iPSC control cells (MSC and LC2) with H2DCFDA, followed by flow cytometric analysis. Results are representative of three independent experiments ±SD. (B) Representative immunofluorescence staining for γH2AX (red) in hESC, iPSC and parental iPSC control cells. Nuclei were counterstained with DAPI (blue, ×1000). (C) The number of γH2AX foci/cell are representative of the mean of three independent experiments ±SD. (D) Representation of cell cycle profile obtained after propidium iodide staining of hESC, iPSC and parental iPSC. (E) Graphic representation of the percentage of live cells in G1 (black bars), S (grey bars) and G2 (white bars) obtained in D. Results are representative of three independent experiments ±SD. *p* values are in text.

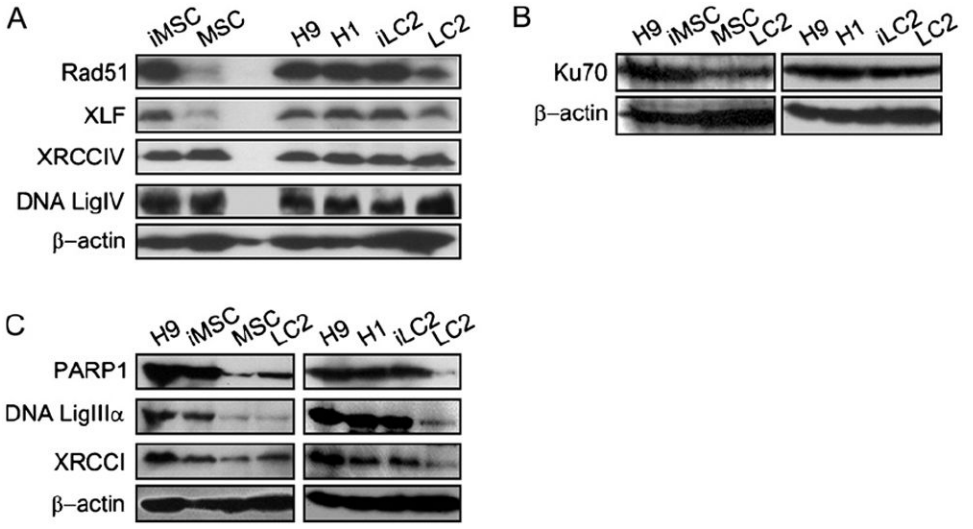

Fig. 2.

Immunoblotting analysis of HR and NHEJ proteins in hESC, iPSC and parental control cells. Immunoblotting analysis of (A) HR protein RAD51, NHEJ proteins XLF, DNA LigIV and XRCCIV, (B) NHEJ protein Ku70, and (C) PARP1, DNA LigIIIα and XRCC1 proteins that participate in BER, SSB and Alt NHEJ pathways was performed in WCE of hESC (H9 and H1), iPSC (iMSC and iLC2), and parental control cells (MSC and LC2). β-Actin was used as loading control.

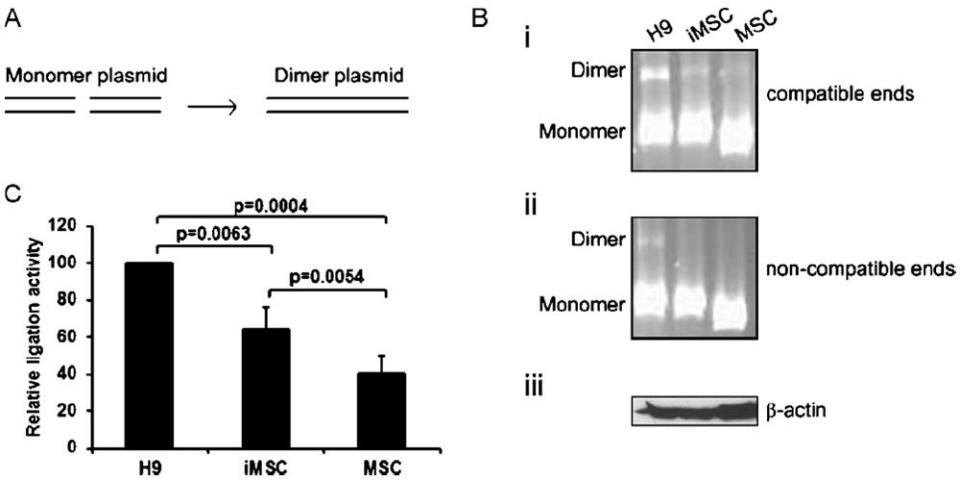

Fig. 3.

In vitro NHEJ assays in hESC, iPSC and parental control cells. (A) Schematic diagram showing ligation of linear plasmid monomers to form plasmid dimers. (B) Representative autoradiographs of agarose gels showing ligation of (i) linearized pUC19 digested with BamHI endonuclease (compatible ends) and (ii) linearized pAcGFP1-N2 with KpnI/SacI (non-compatible ends), following incubation in WCE from H9, iMSC and MSC. (iii) Representative immunoblot of β-actin level in the three different WCE used for *in vitro* NHEJ presented in (Bi). (C) Graphic representation of relative ligation activity in H9, iMSC and MSC. Results are representative of three independent experiments ±SD. *p* values are shown.

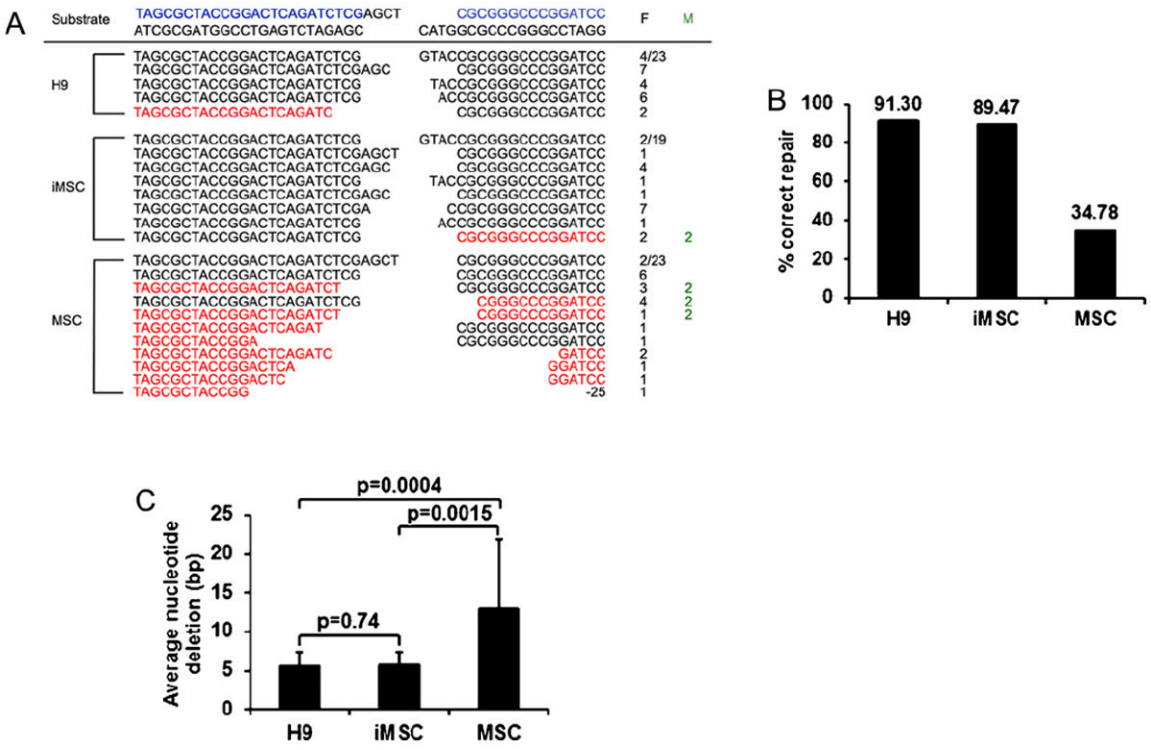

Fig. 4.

Sequencing of DSB repair junctions in hESC, iPSC and control cells. (A) DNA sequence of DSB repair junctions were obtained after ligation of non-compatible ends linearized (Kpn1/SacI) plasmids in H9, iMSC and MSC. The occurrence of a given sequence (F) is indicated in black. Microhomologies (≥2 bp, M) found at the repair junction are indicated in green. Intact DNA sequence adjacent to the single strand overhang in the substrate is indicated in blue. Junctions with deleted sequences beyond the single strand overhang are considered inaccurate and shown in red. (B) Percentages (mean values and SD) of accurate junctions in clones from each set of experiments depicted in (A). (C) Graphic representation of the mean nucleotide loss in inaccurate junctions observed in plasmids recovered from H9, iMSC and MSC *in vitro* NHEJ. (For interpretation of the references to color in this figure legend, the reader is referred to the web version of the article.)

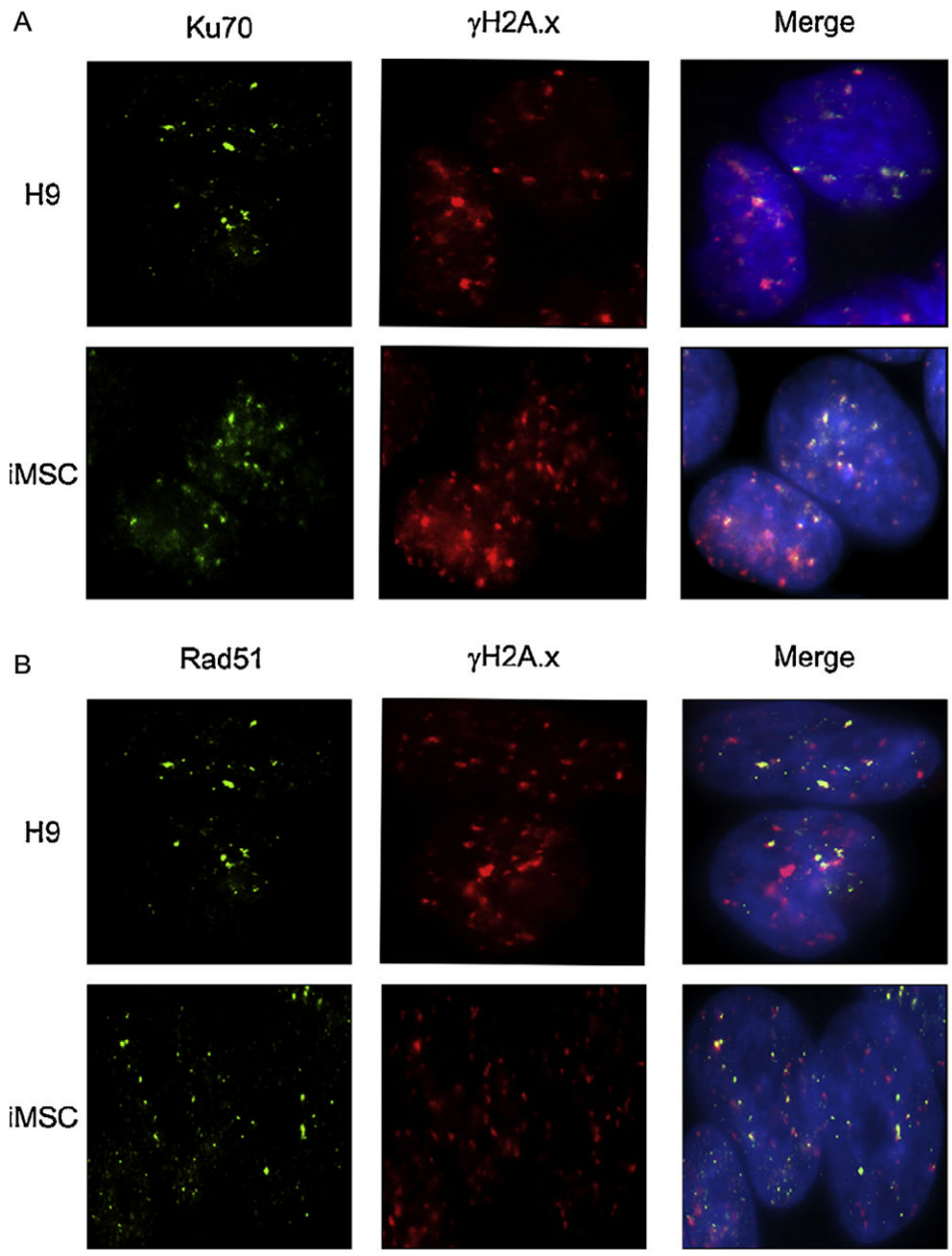

Fig. 5.

Co-immunostaining for γH2AX and DSB repair proteins in hESC and iPSC after DNA damage induction. (A and B) Representative immunofluorescence staining for (A) γH2AX and Ku70 and (B) γH2AX and RAD51 in H9 and iMSC following 5 Gy 4 h irradiation. Cells were immunostained for Ku70 or RAD51 (green, left panel) and coimmunostained for γH2AX foci (red, middle panel). Right panel shows merged fluorescence patterns with co-immunostained regions in yellow. Nuclei are counterstained with DAPI (blue, ×1000).

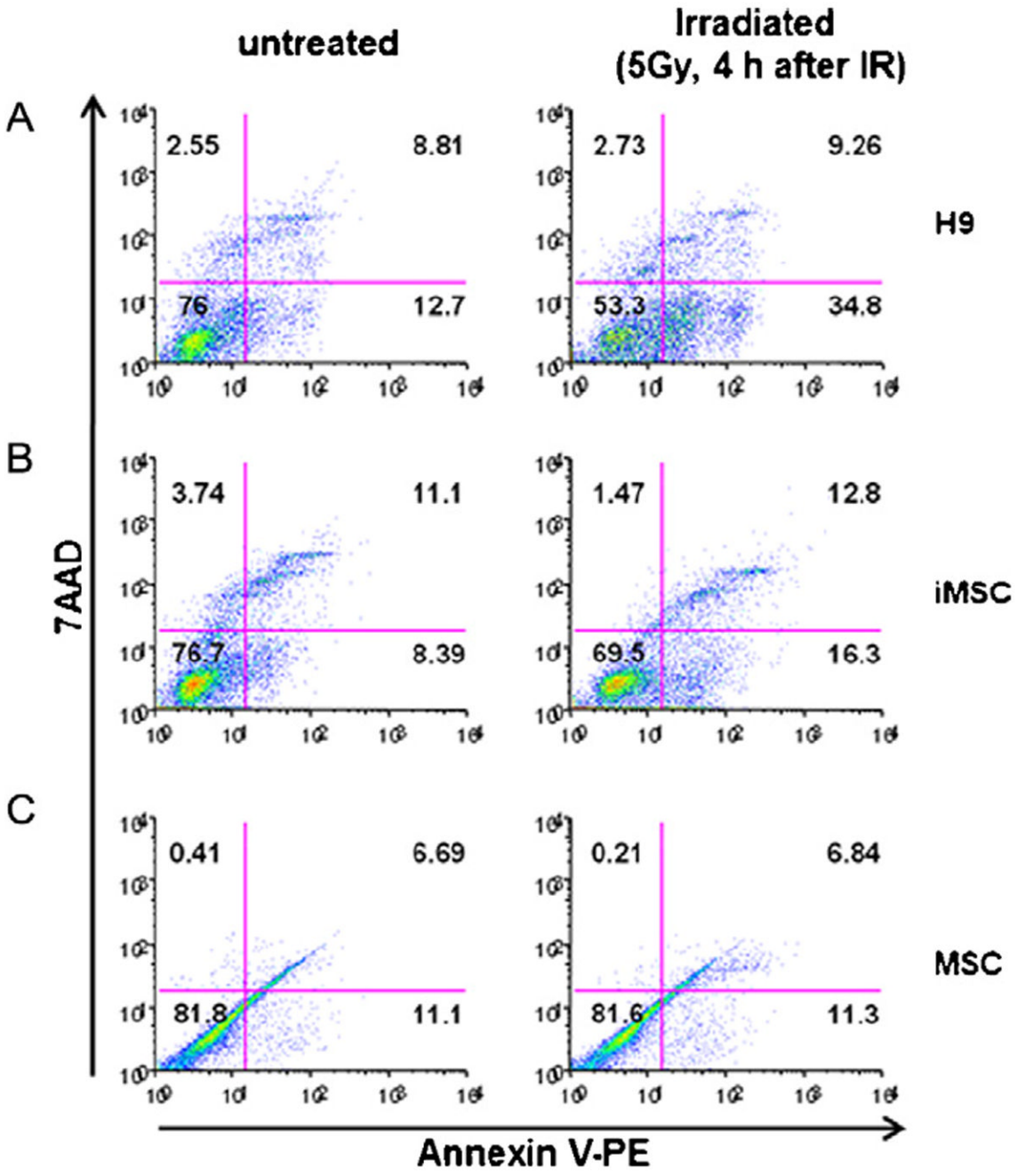

Fig. 6.

Flow cytometric analysis of Annexin IV in irradiated hESC, iPSC and control cells. Representative dot blot of apoptotic cells detected by Annexin V–PE binding and 7AAD labeling in (A) H9, (B) iMSC and (C) MSC cells after the indicated times of irradiation (IR). Apoptotic cells in the lower right quadrant, necrotic cells in the upper right quadrant, and viable cells in the lower left quadrant were detected and the percentage of each population is presented.

Table 1

Quantification of γH2AX foci and RAD51 or Ku70 co-localization in hESC and iMSC cells following γ irradiation.

	1 Gy	γH2A.x foci/cell	Rad51/γH2A.x (%)	Ku70/γH2A.x (%)
H9	0	7.8	0.0	0.0
	20 min	11.6	10.7	10.7
	2 h	93.5	17.3	29.2
	4 h	71.9	10.0	31.8
iMSC	0	6.5	0.0	0.0
	20 min	15.4	2.8	3.0
	2 h	68.8	7.9	27.7
	4 h	75.5	8.3	20.8

At least 50 cells were analyzed per treatment.